Article

Mapping Spatiotemporal Heterogeneity in Multifocal Breast Tumor Progression by Noninvasive Ultrasound Elastography-Guided Mass Spectrometry Imaging Strategy

Peng Zhou,[¶] Yu Xiao,[¶] Xin Zhou, Jinghui Fang, Jingwen Zhang, Jianjun Liu, Ling Guo, Jiuhong Zhang, Ning Zhang, Ke Chen, and Chao Zhao*

Cite This: JACS Au 2024, 4, 465−475

Read Online

ACCESS | 📊 Metrics & More | 📖 Article Recommendations | Ⓢ Supporting Information

ABSTRACT: Spatiotemporal heterogeneity of tumors provides an escape mechanism for breast cancer cells, which can obstruct the investigation of tumor progression. While molecular profiling obtained from mass spectrometry imaging (MSI) is rich in biochemical information, it lacks the capacity for in vivo analysis. Ultrasound diagnosis has a high diagnostic accuracy but low chemical specificity. Here, we describe a noninvasive ultrasound elastography (UE)-guided MSI strategy (UEg-MSI) that integrates physical and biochemical characteristics of tumors acquired from both in vivo and in vitro imaging. Using UEg-MSI, both elasticity histopathology metabolism "fingerprints" and reciprocal crosstalk are revealed, indicating the intact, multifocal spatiotemporal heterogeneity of spontaneous tumorigenesis of the breast from early, middle, and late stages. Our results demonstrate a gradual increase in malignant degree of primary focus in cervical and thoracic mammary glands. This progression is characterized by increased stiffness according to elasticity scores, histopathological changes from hyperplasia to increased nests of neoplastic cells and necrotic areas, and regional metabolic heterogeneity and reprogramming at the spatiotemporal level. De novo fatty acid (FA) synthesis focused on independent (such as ω-9 FAs) and dependent (such as ω-6 FAs) dietary FA intake in the core cancerous nest areas in the middle and late stages of tumor or in the peripheral microareas in the early stage of the tumor. SM-Cer signaling pathway and GPs biosynthesis and degradation, as well as glycerophosphoinositol intensity, changed in multiple characteristic microareas. The UEg-MSI strategy holds the potential to expand MSI applications and enhance ultrasound-mediated cancer diagnosis. It offers new insight into early cancer discovery and the occurrence of metastasis.

KEYWORDS: spatiotemporal heterogeneity, breast tumor progression, ultrasound elastography-guided mass spectrometry imaging, mass spectrometry imaging, metabolic reprogramming
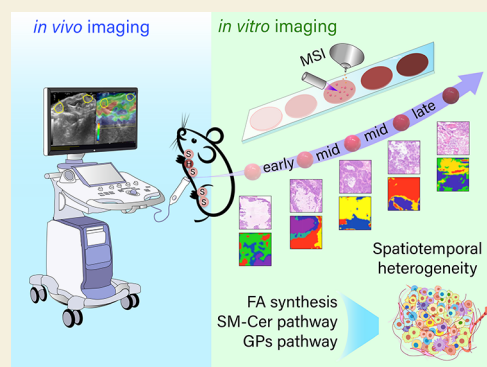
1. INTRODUCTION

Breast cancer is a frequent heterogeneous disease on a molecular level, with the emphasis being placed on multiple primary and metastasis focuses on investigating or predicting the tumor pathogenesis and response to therapy.[1,2] Tumor heterogeneity, both spatial and temporal, can exist at various molecular levels (such as genome, epigenome, metabolome, lipidome, and proteome) and has significant clinical implications, usually associated with a long-term adverse outcome throughout a stage of tumor growth.[3−6] This situation is caused by multiple interactions through the complex intra- and/or intercellular processes, leading to various molecular phenotypes and different histopathological subtypes appearing in the same lesion.[3−6] This complex information is poorly understood, which interrupts our ability to investigate the molecular mechanism of tumor progression and specific diagnosis and effective treatment. Considering the complex spatiotemporal variations in tumor and its micro-

environment, it is widely appreciated that exploring these data at multiple spatiotemporal points gives far superior diagnosing capability for different tumor progression and resistance mechanisms and eventually aims to predict tumor proliferation, malignancy, and metastasis.[7,8]

Mass spectrometry-based multiomics techniques measure the phenotype, protein, and metabolite profiles in homogenized tissues or cells, but they do not capture the significant variations of spatial information, thus limiting their use for accurate diagnosis and personalized medicine.[9,10] Mass spectrometry imaging (MSI) technique, namely label-free in
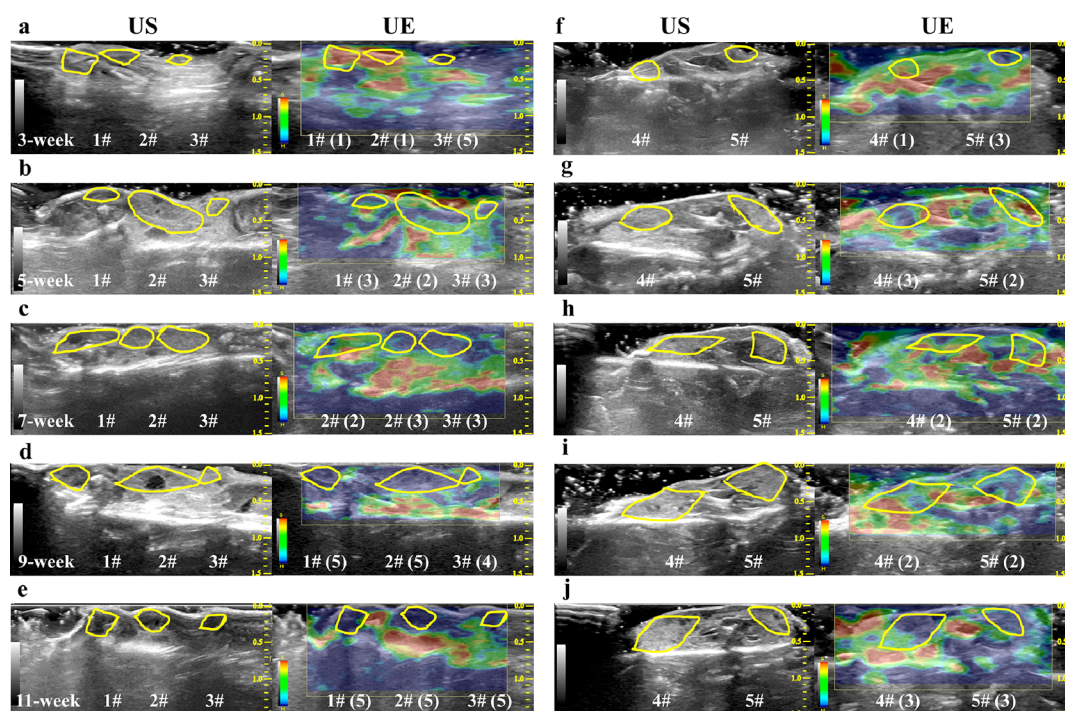
Figure 1. Representative ultrasound (US) and UE images from multifocal animal model during breast tumor progression. (a−e) US (left side) and UE (right side) results from the 1#, 2#, and 3# primary focuses of cervical and thoracic mammary gland; (f−j) US (left side) and UE (right side) results from the 4# and 5# primary focuses of abdominal and inguinal mammary glands. "S" from the color bar of UE represents soft (red), and "H" represents hard (blue). The numbers from brackets in UE images represent the elasticity score of tumor. More details about elasticity score on a five-point scale are indicated in Section 4.2.

situ imaging, offers unbiased visualization and direct profiling of diverse endogenous molecular species and exogenous substances on a single or serial tissue sections and thus provides a more accurate strategy clearly for mapping tumor heterogeneity by clustering the molecular signatures in the region of interest (ROI), which includes the cancerous, invasive, or stromal areas.[11−15] Santoro et al. applied the specific metabolomics profiling sourced from MSI to characterize the invasive breast cancer (IBC), ductal carcinoma in situ (DCIS), and various other molecular subtypes of breast cancer. For example, antioxidant molecules and lipids with higher degrees of saturation contribute to identifying IBC and lipids associated with inflammatory, and apoptotic signaling regulation appears to have essential roles in distinguishing between DCIS and IBC.[14] Kawashima et al. found that the fatty acid (FA) composition and spatial distribution of phosphatidylinositols (PIs) are associated with invasion and metastasis of breast cancer by combining the MSI and transcriptomic analysis. Specifically, significant accumulations of PIs-containing polyunsaturated fatty acid (PI-PUFA), such as PI (18:0/20:4), exhibit in normal ductal cells, whereas accumulations of PIs-containing monounsaturated fatty acid (PI-MUFA) show in noninvasive cancer cells.[15]

Heterogeneity analysis in the bulk of the previous strategy is unable to perfectly reconcile the variability and correlation of multisource information at multiple primary focuses simultaneously, such as physical, biological, and pathological properties. Additionally, it has also been hard to achieve complete phenotype variation by individual biopsies methods of tumor. Practicability of a noninvasive strategy for monitoring the spatiotemporal heterogeneity or predicting the molecular response to external stimuli at an early stage of tumor would facilitate the design of personalized therapy and allow the exploration of molecular mechanisms in breast tumor progression. Ultrasound imaging is one of the most effective and convenient methods that combine molecular imaging and ultrasound medicine with unique superiorities, including noninvasiveness, safety, repeatability, and accuracy. Among them, ultrasound elastography (UE) is an emerging ultrasound-based modality for in vivo imaging that has been used for visualization of tissue elasticity.[16−18] In addition to variations of biomolecular expression, elasticity or stiffness of tumor tissues is also an important "physical" marker to distinguish malignant tumors from normal or stromal tissues.[18] Compared to the current standards of B-mode ultrasound and aspiration biopsy approach, differentiating the various benign or malignant tumors using UE proves to have more outstanding performance in tumor location and diagnostic accuracy for breast,[19−21] thyroid, and prostatic lesions analysis.[22,23] It is reported that the UE technique is used for prognostication of neoadjuvant chemotherapy response in different models with high specificity, providing a great potential for active detecting of tumor response to drug treatment, such as locally late-stage breast cancer as early as 2 weeks into treatment,[19] IBC,[20] and murine breast cancer model treated by chemotherapy.[21]

Molecular profiling sourced from MSI is abundant but lacks the power to perform in vivo analysis. UE diagnosis has relatively low chemical specificity but high diagnosis precision. The strengths and weaknesses of MSI and UE, as well as the important functions in early discovery and continuous check of cancers or diseases, make them highly complementary when combined for multimodal imaging of multimolecule characteristics. Thus, by using noninvasive UE to guide and extend the

specificity of MSI, we focus on the spatiotemporal heterogeneity in multifocal breast tumor progression: (a) how intra/intertumor heterogeneity at different growth stages can be analyzed from UE data and (b) how spatial distribution of metabolites and its pathway data can be used to better understand the molecular mechanisms of tumor progression. Correlating heterogeneous features in physical and biochemical level, including tissue stiffness, cellular morphology, and molecular distribution, can provide insights that may prominently improve therapeutic interventions of tumor.

2. RESULTS AND DISCUSSION

To analyze the progression characteristics of breast tumor and further investigate the spatiotemporal heterogeneity, we selected a transgenic mouse model, namely mouse mammary tumor virus (MMTV) promoter-driven polyoma middle T oncogene (PyMT) model, that accurately recapitulates progressive stages of spontaneous tumorigenesis similar to human breast cancer and its metastasis.[24,25] As the stepwise progression of MMTV-PyMT tumors, cancer cells and associated stromal microenvironment undergo various molecular variations, such as upregulated ErbB receptor family members, significant changed immune cell infiltration and extracellular matrix (ECM) composition, and malignant lesions of mammary epithelial cells, leading to the rapidly progressive breast cancer with multifocal tumors.[26] However, it is unclear how to investigate and understand spatiotemporal heterogeneity features and molecular metabolism in complex multifocal breast tumor progression.

2.1. UE-Based Noninvasive Tumor Monitoring

We use UE as a noninvasive approach to explore physical characteristic of breast tumor (such as stiffness) and construct the correlations between malignant progression of breast tumors and stiffness variation in both single and multifocal tumors. Briefly, tissue elastic characteristics change with the variation of the tissue fibrosis degree. Various breast diseases have different biomechanical features due to the obvious differences in the structure and types of fibrous tissue.[16−18,27] UE is based on the generation of strain by an axial or longitudinal compression into the targeted tissues. After compression, ultrasonic echo signals are acquired, then the extent of strain is determined by estimating the variation of displacement in the internal tissues.[16−18,27]

According to the tissue stiffness changed significantly in the multifocal tumor models by using UE methodology, the results indicate that the spatiotemporal heterogeneity during tumor progression existed in three aspects, including the morphological variation accompanied by a development from cystic to solid tumors according to semiquantitative SR measurements, the degree of malignant lesions according to the elasticity scores, as well as the differences of tumor growth rate in interprimary focus (Figures 1 and 2).

We selected early (3 weeks), middle (5 and 7 weeks), and late stage (9 and 11 weeks) to comprehensively simulate the progression of breast cancer.[24−26] To be more specific, representative UE and ultrasound images of breast tumor show that the stiffness of tumors increases gradually in the 1# and 2# primary focuses of cervical and thoracic mammary glands during the tumor progression according to the SR measurements (Figure 2a), which is characterized by the transition from cystic to solid tumors and increased malignant degree according to elasticity scores (variation from 1 point to
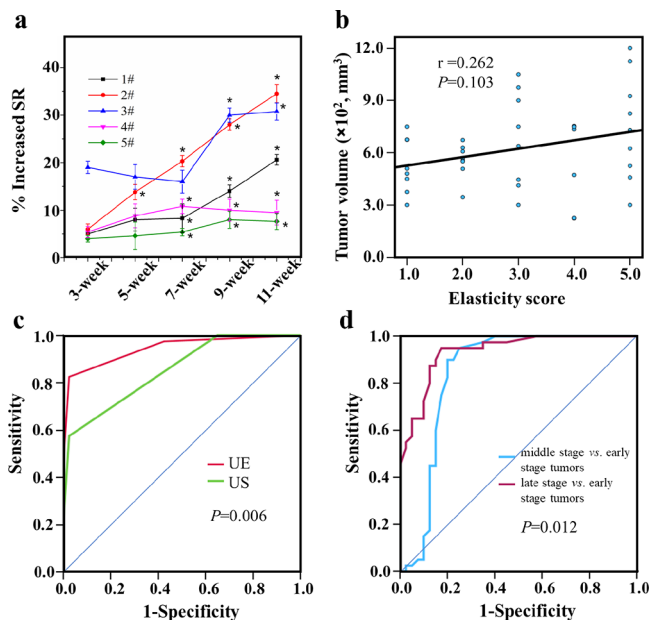
Figure 2. Evaluation of the UE strategy. (a) Increase of SR from baseline on five primary focuses during tumor progression ($n = 40$). The SR value 3 weeks ago is set to baseline. % Increased SRs for each group are calculated by using means ± standard error of the means. (b) Correlation between elasticity score and tumor size in tumor progression, Spearman's correlation coefficient test ($n = 40$). (c) ROC curves for UE and ultrasound (US) in differentiating tumors mainly composed of glandular cavity (score 1−3, $n = 40$) from tumors with a high degree of malignant (score 4 or 5, $n = 40$). (d) ROC curves of classification results for different progression stages of breast tumor, including middle-stage ($n = 40$) vs early-stage tumors ($n = 40$) and late-stage ($n = 40$) vs early-stage tumors ($n = 40$). *$P \leq 0.05$.

5 points during 3−11 weeks) (Figure 1a−e). By contrast, the breast tumors located in abdominal and inguinal mammary glands (4# and 5# primary focuses) do not increase characteristics in elasticity changes (Figure 2a; elasticity scores 1−3 from Figure 1f−j), which show that the heterogeneity of growth rate is existed between intertumors. In addition, elasticity scores are not correlated with tumor sizes during the tumor progression ($r = 0.262$, $P = 0.103$, Figure 2b), which indicates that a single variation in tumor sizes cannot accurately judge a trend of tumor progression and also demonstrates that the UE technique is helpful to continuously monitor the multiple primary tumors and metastasis.

In order to evaluate the feasibility and accuracy of using the UE strategy to help diagnose breast tumors, the receiver operating characteristic (ROC) curves are used for two different methods, UE and conventional B-mode ultrasound (Figure 2c), in distinguishing the cystic and solid tumors. The area under the curve (AUC) for UE (0.944) is significantly higher than that for B-mode (AUC = 0.852, $P = 0.006$) (Figure 2c). To further investigate the performance of UE for different progressing stages of tumor, ROC curves are generated at early and middle (3, 5, and 7 weeks) and late stages (9 and 11 weeks). AUV are 0.846 and 0.935 for tumors from middle-stage vs early-stage tumors, and late early and middle stage vs late stage ($P = 0.012$) (Figure 2d). Above results demonstrate that the UE technique can achieve high accuracy, which is significantly superior to the conventional ultrasound classification in breast tumor progression.
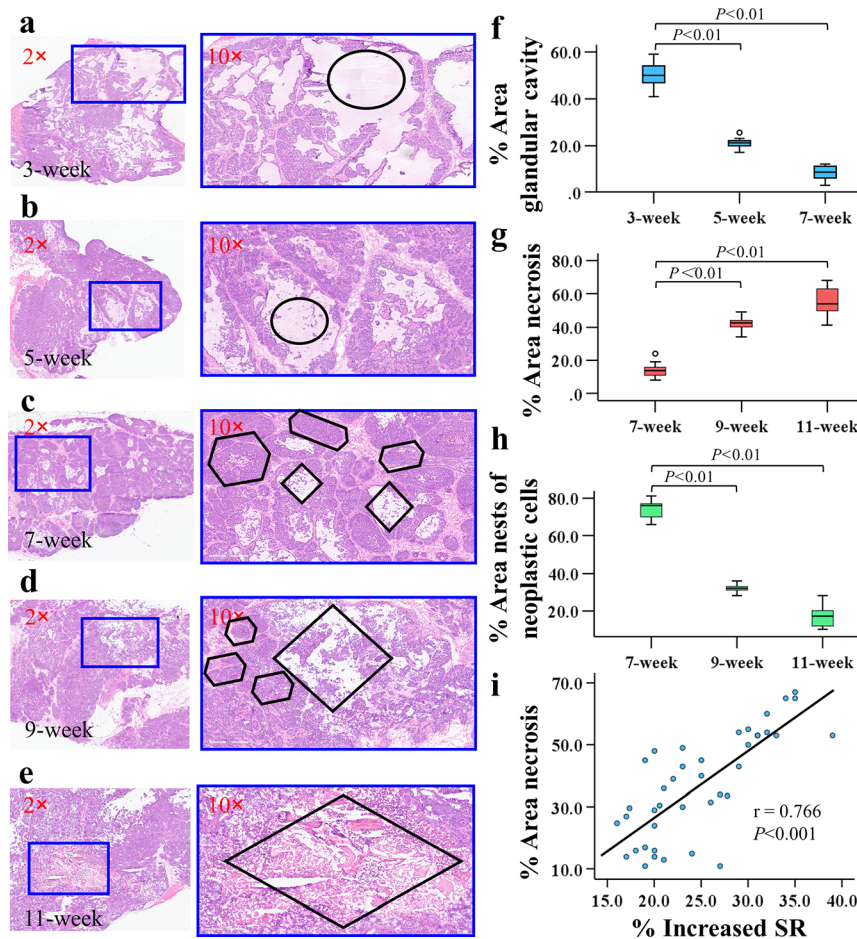
Figure 3. Representative histopathological characteristics during breast tumor progression (a−e) and related statistical analysis of characteristic microareas in 2# primary focus (f−i). Box plots show a statistically significant ($P < 0.01$) decrease in % area glandular cavity (f, $n = 40$) and nests of neoplastic cells (h, $n = 40$), as well as increase in % area necrosis (g, $n = 40$) during tumor progression. (i) Correlation between % area necrosis and % increased SR in tumor progression. Spearman's correlation coefficient test ($n = 40$). Representative areas including glandular cavity, necrosis, and nests of neoplastic cells show using black circles, diamond, and hexagon, respectively.

Thus, noninvasive UE provides a crucial guidance for exploring the distinct variation in physical characteristics for tumor progression, which is manifested in the following points: (1) compared to in vitro method, it has obtained the in vivo distribution and morphological variations of tumors at different growth stages of multiple lesions, which help us to accurately select samples from the tumor models for downstream analysis, effectively reduce the amount of animal model and save time. (2) Compared with B-mode ultrasound, UE provides multiple information on tumor and associated tissue and nodules, such as in vivo visualization, location, and malignant degree. Additionally, UE and B-mode testing methods complement each other and verify each other, which effectively improves the operability of methods.

2.2. Correlation Analysis of UE and Histopathological Progression of Breast Tumor

To validate UE as a guiding function for the heterogeneous investigation of tumor at the spatiotemporal level, we further introduced morphological analysis and constructed the correlation between UE and morphological variation for tumor progression. Based on the available UE guidance (Figures 1 and 2), the tumors located in the thoracic mammary gland (2# primary focus), which allows the potential factors in increased malignant degree according to SR on

elastography and elasticity scores are selected for further studies.

Figure 3a−e summarizes the intra/intertumor heterogeneity-related cellular characteristics and distribution of histopathological types at five points in time of tumor progression in 2# primary focus. During the 3 weeks of breast tumor progression, cells are arranged in an irregular glandular cavity, accompanied by significant hyperplasia. Peripheral tumor cells are arranged in a papillary manner. Along with the time extension for tumor progression, the area of the glandular cavity trended to reduce gradually from 3 to 7 weeks with statistically significant ($P < 0.01$) (Figure 3f). The results suggest that a large proportion of glandular cavity (Figure 3f) is likely to contribute to the lower stiffness at early stage of tumor growth (Figure 1a−c). At 7 weeks of tumor progression, distributions of neoplastic cells with higher density replace the glandular cavity with a loose construction. With the rapid malignant development of breast lesions, nests of neoplastic cells fuse into pieces with increased neoplastic cell density (Figure 3b,c). It is notable that the infiltration of cancerous cells into the peripheral stroma of mammary gland results in the mixed and dispersed distribution of these microareas. Fused glandular cavities display the nest-/sieve-like arrangement, and tumor coagulative necrosis appears in the center of nests of neoplastic cells as the day progresses. Specifically, at 7 weeks of tumor progression, we observe the

presence of central necrotic areas in nests of neoplastic cells (Figure 3c) and find that the proportions of necrotic areas increase significantly (Figure 3g), while nests of neoplastic cells decrease from 7 to 11 weeks (Figure 3h), which is a major feature of aggressive breast cancers and closely linked to poor prognosis. More importantly, increased SR positively correlates with histological features ($r = 0.766$, $P < 0.001$, according to the variation of necrotic areas, Figure 3i). This again demonstrates a close correlation between cellular morphology and tissue stiffness.

2.3. Spatiotemporal Heterogeneity of Tumor Progression Using UEg-MSI

According to the increased elasticity scores and histopathological features, we find that the malignant degree increases with the transition from cystic to solid tumors during progression in primary focuses of cervical and thoracic mammary gland (Figures 1−3). It is reported that an increase in tumor stiffness further activates the signal pathways associated with proliferation and invasion of neoplastic cells, which can change the ECM and cellular reprogramming and heterogeneity. These processes require metabolism for both the energy generation and synthesis of signaling molecules, implicating a potential reciprocal crosstalk between physical characteristics (such as stiffness, mechanical forces, etc.) and molecular metabolism.[28] Among them, the variation of lipid composition, namely the first potential indicator of phenotypic changes, occurs much faster than the variation of protein or gene expressions.[29,30] We propose that stiffness variation during tumor progression may be linked to specific molecular signaling and tumor composition remodeling. To confirm our hypothesis, MSI is introduced to acquire molecular fingerprint features of breast tumor metabolism at the spatiotemporal level.

Among breast tumor progression, 2# primary focus located in thoracic mammary gland is selected based on real-time UE monitoring and histopathological identification. To understand intra/external-tumor heterogeneity from molecular level and investigate the metabolic features of tumor progression, the spatial segmentation of tumor samples sourced from MALDI imaging coupled with laser postionization (MALDI-2) data is performed using SCiLS Lab software. MALDI-2 with the trapped ion mobility spectrometry function can provide important support revealing the complex spatial distribution and composition of metabolites and lipids. Compared to organ identification with some spatially contiguous ROIs, tumor samples are featured by the multiple sporadic ROI arrangements and morphology.[31,32] Thus, the top two or three clusters of mass spectra are screened to show metabolic similarity and heterogeneity during tumor progression (Figure 4). By combining histological annotation, some representative microareas from tumor samples present different colors are defined and coregistered during tumor progression, to be more specific, glandular cavity ("gc" from Figure 4a), hybrid hyperplasia ("hy+gc" from Figure 4a) and carcinoma areas ("c" from Figure 4a) in 3-week-group, glandular cavity ("gc" from Figure 4b) and carcinoma areas ("c1, c2" from Figure 4b) in 5-week group, nests of neoplastic cells ("nc" from Figure 4c) and glandular cavity areas ("gc" from Figure 4c) in 7-week group, nests of neoplastic cells ("nc" from Figure 4d,e) and necrotic areas ("n" from Figure 4d, e) in 9- and 11-week group. Using probabilistic latent semantic analysis (pLSA) with deterministic initialization, these representative microareas
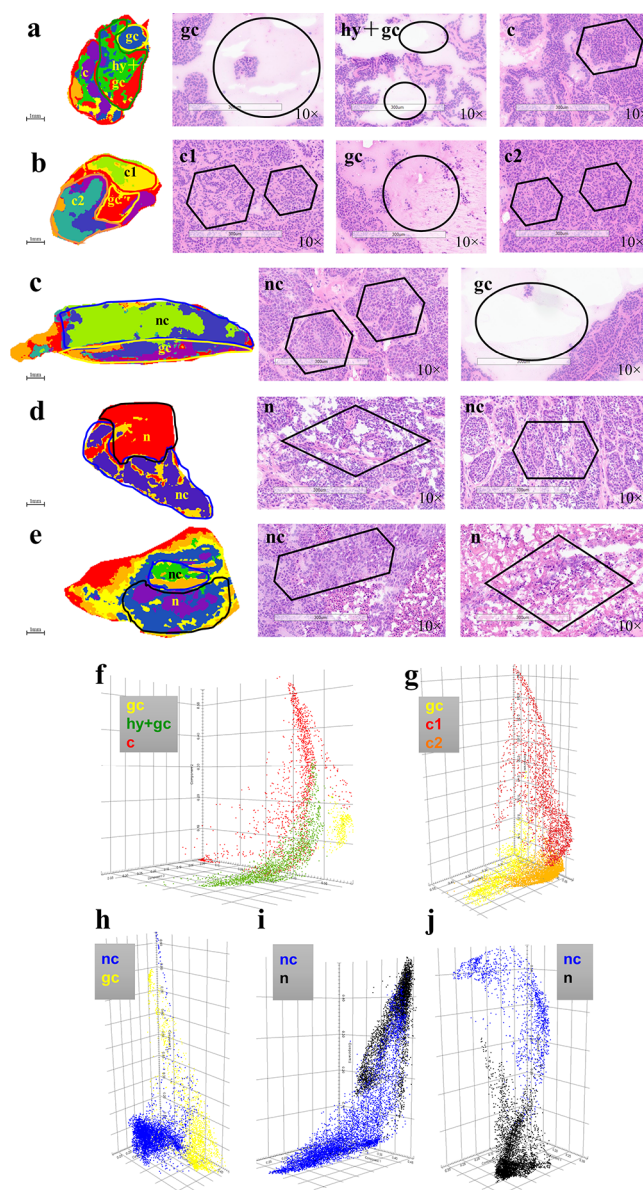

Figure 4. MSI data analysis during breast tumor progression in 2# primary focus. (a−e) Spatial segmentation and corresponding histopathological characteristics of microareas. Glandular cavity (gc; black circle), hybrid hyperplasia (hy+gc; black circle), carcinoma area (c; black hexagon), carcinoma areas (c1 and c2; black hexagon), nests of neoplastic cells (nc; black hexagon), and necrotic areas (n; black diamond). (f−j) Metabolic heterogeneity of intratumors by using pLSA score plots. $n = 6$. Scale bar, 1 mm.

are well distinguished from each other for verifying the metabolic heterogeneity of intratumors (Figure 4f−j).

To further analyze the metabolic heterogeneity of intertumors and discover spatial distribution variation of characteristic molecules associated with tumor progression, we perform component analysis by using pLSA with six components at 95% confidence intervals in four groups including 5 vs 3 weeks, 7 vs 3 weeks, 9 vs 3 weeks, and 11 vs 3 weeks, then acquire the tumor progression-related metabolites with significant differences and quantitative results (Figures S1−S5; Table S1). The results also demonstrate that the metabolome and lipidome of breast tumors are disturbed significantly to cope with the increased malignancy from 3 to

11 weeks, manifesting a clean separation of four pairwise groups including 5 vs 3 weeks, 7 vs 3 weeks, 9 vs 3 weeks, and 11 vs 3 weeks (Figure S1).

The ion images obtained from MALDI-2 display the high heterogeneity in the spatial distributions of two species of endogenous molecules, including metabolites (glycerophosphoinositol) and lipids (fatty acids [FA], phosphatidic acids [PA], ceramides [Cer], ceramide 1-phosphates [CerP], sphingomyelins [SM], lysophosphatidic acids [LPA], phosphatidylethanolamine [PE], lysophosphatidylethanolamines [LPE], phosphatidylinositols [PI], lysophosphatidylinositol [LPI], phosphatidylserines [PS], lysophosphatidylglycerol [LPG]) throughput tumor progression (Figures 5, 6, S3 and S4, and Table S1).
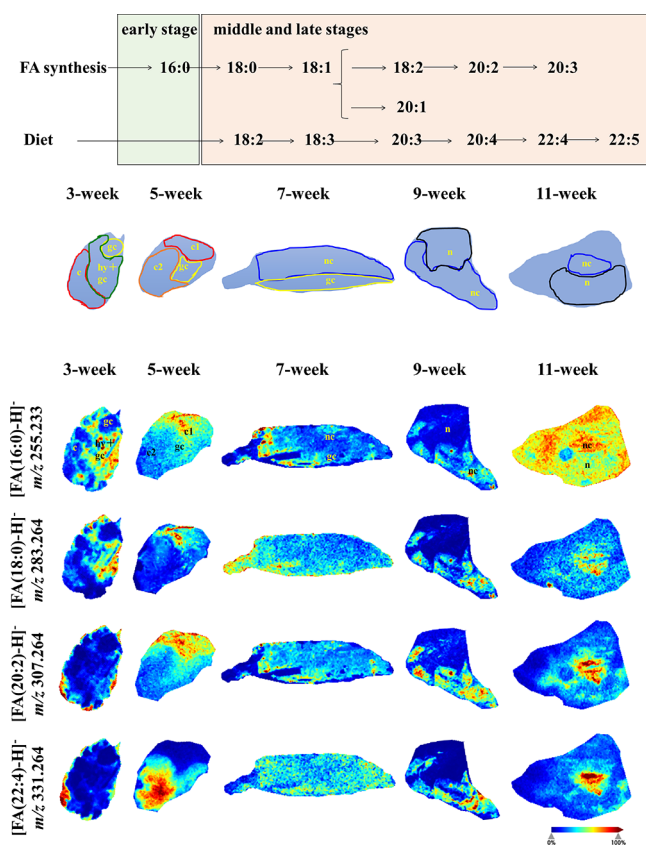

Figure 5. FA synthesis pathway and spatiotemporal heterogeneity of related FA during breast tumor progression in 2# primary focus. The schematic diagram reveals the synthesis pathways and critical products from de novo FA synthesis, including the independent (such as ω-9 FAs) and dependent (such as ω-6 FAs) of dietary FA intake. Arrows are used to indicate the elongation or desaturation steps. Abbreviations in the MSI images indicate the different microareas detected by MALDI-2, such as glandular cavity (gc), hybrid hyperplasia (hy+gc), carcinoma area (c), carcinoma areas (c1 and c2), nests of neoplastic cells (nc), and necrotic areas (n). n = 6. Scale bar, 1 mm (the same below). More spatial distributions of FAs are shown in Figure S3.

Among them, the spatial distribution of glycerophosphoinositol shows an increasing trend of metabolic heterogeneity in early and late stages of tumor progression. More specifically, upregulated glycerophosphoinositol is concentrated in hybrid hyperplastic and glandular cavity areas for 3-week-tumor, as well as the nest areas of neoplastic cells for 9 and 11 weeks
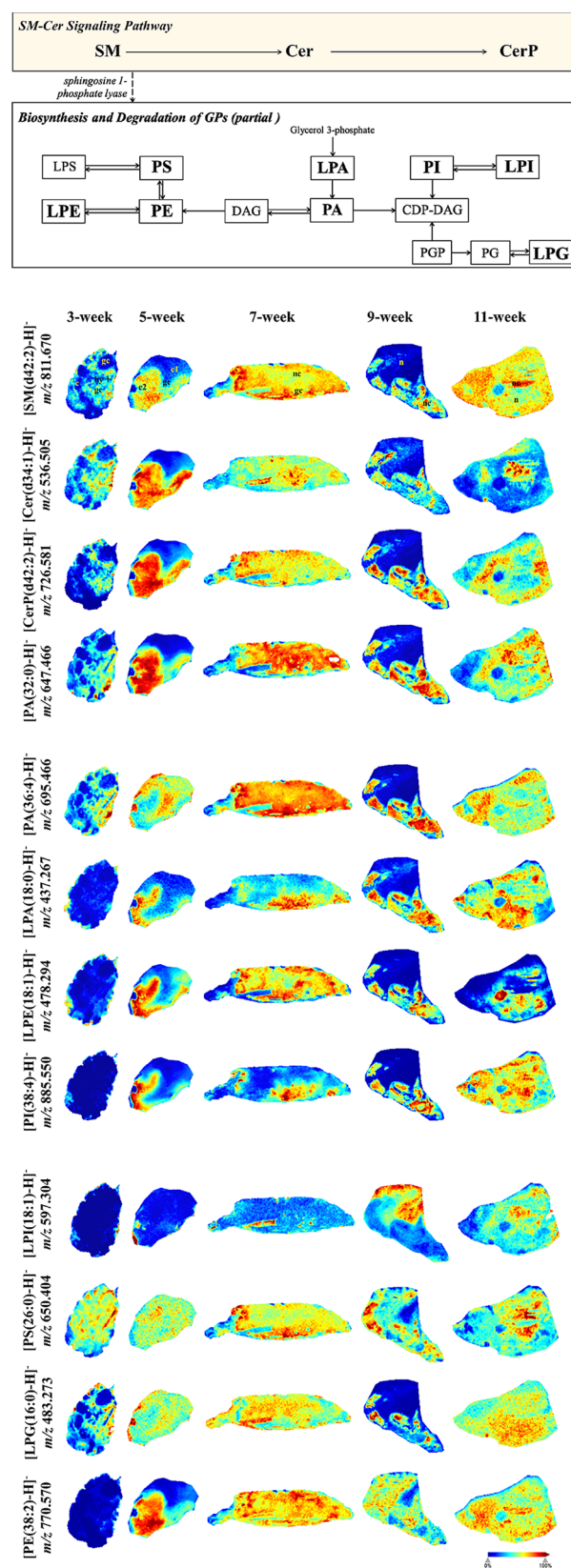

Figure 6. SM-Cer signaling pathway and biosynthesis, degradation pathway of GPs (partial), and spatiotemporal heterogeneity of related lipids during breast tumor progression in 2# primary focus. Arrows are used to indicate the elongation or desaturation steps. The bold lines represent the detected lipids. More spatial distributions of lipids are shown in Figure S3.

(Figure S3). There is a significant increase in normalized intensities of glycerophosphoinositol in nests of neoplastic cells during the tumor progression using quantitative analysis (Figure S4). Starting from membrane phosphoinositides, glycerophosphoinositol formation is performed under the activities of phospholipase A$_2$ and lysolipase after corresponding lysophosphoinositide generation with arachidonic acid release. Glycerophosphoinositol and its metabolic pathways are known to have important functions in various cellular events, such as proliferation, motility, and invasion for carcinoma cells.[33,34] The normalized intensity of glycerophosphoinositol in aggressive areas of neoplastic cells is higher than in the necrosis areas during 9 and 11 weeks of progression (Figures S3 and S5), suggesting that more aggressive tumors are featured by lower glycerophosphoinositol consumption, and this variation is consistent with a previous report that describes intracellular concentrations of glycerophosphoinositol can change upon oncogenic transformation and cell differentiation by autocrine and/or paracrine mechanisms.[34,35]

It is further observed that FAs and PAs present different spatial distributions according to the different carbon chain lengths of unsaturated FAs during tumor progression. The hybrid hyperplastic and glandular cavity areas dominated by saturated FA(16:0) and FA(18:0) showed high expression in the early stage compared to all other FA species. In addition to FA(16:0) and FA(18:0), cancerous (c1 or c2 from 5 weeks), nests of neoplastic cells (nc from 9 or 11 weeks) contributed by upregulated FAs are observed in the middle and late stages compared to the early stage of tumor. Specifically, inspections of the spatial distribution of individual ions confirm that there is a heterogeneous distribution of unsaturated FA species within the cancerous areas dominated by C18, C20, and C22 of FAs in middle stage, as well as the nest areas of neoplastic cells dominated by them in late stage of tumor progression. Compared to the spatial distribution of FAs, PAs exhibit a significant heterogeneity at an early stage within upregulated expression concentrated in the hybrid hyperplastic and glandular cavity areas. Additionally, it is observed that differences in spatial distributions sourced from C32 of PA exist from early to late stages and C36 and C38 of PA in early and late stages of tumor progression (Figures 6 and S3).

FA species (20:2/3) are produced by the synthesis pathway from essential linoleic acids (Omega 6) [FA(18:2)] and α-linoleic acids (omega 3) [FA(18:3)] to arachidonic acid [FA(20:4)]. As the intermediate species of FA synthesis, they are characterized as nonproductive accumulation.[36,37] Upregulated FA(20:2/3) during tumor progression demonstrates a significant preference for de novo lipid synthesis. During tumor progression, various cancer cells use de novo synthesized FAs to produce excessive biomass for cell proliferation. By using real-time qPCR, the transcript abundance values of FA synthase (Fasn) increase by 5.1-fold in 5-week vs 3-week groups, 3.5-fold in 7-week vs 3-week groups, 4-fold in 9-week vs 3-week groups, and 5.9-fold in 11-week vs 3-week groups (Figure S6). Upregulated Fasn has been displayed in various cancer (sub)-types and is closely associated with a poor prognosis.[38] We also describe the major pathways of FA species generation from the spatiotemporal analysis based on MSI images (Figure 5), with the characteristic microareas of tumor progression where FA species reveal an upregulated expression signal in situ. Correlating the spatiotemporal features of FA species with their synthesis pathways in tumor progression suggests that all of the FA detected in the breast

tumor samples are generated by *de novo* FA synthesis including the independent (such as ω-9 FAs) and dependent (such as ω-6 FAs) of dietary FA intake. The results also demonstrate that spatiotemporal disturbance of endogenous FAs occurs almost in the core cancerous nest areas in the middle and late stages, not in the peripheral microareas of the tumors (such as necrotic areas, etc.). Additionally, FA species with fully saturated lipid (e.g., FA16:0, FA18:0) are localized to the peripheral microareas (e.g., hybrid hyperplastic and glandular cavity areas) of tumors in early stage. These results are in most cases correlated with the reduction of the membrane permeability to drugs.[36,37] Rysman et al. reported that the cancerous and necrotic areas containing upregulated FA species with various degrees of unsaturation have been shown to occur during tumor progression. This situation could improve the fluidity of the cellular membrane, which is necessary for proliferation and invasion of cancer cells.[39]

In addition to FA and PA species, we also draw the metabolic pathway of some lipids including detected SM, Cer, LPA, LPE, PI, LPI, and PS species, as well as single CerP(d42:2), LPG (16:0) and PE (38:2), which exhibit relatively consistent spatiotemporal features independent of carbon chain length and unsaturated degrees of lipids (Figure 6). We observe that Cer, CerP, and SM are upregulated in hybrid hyperplastic and glandular cavity areas on 3 weeks, one of the cancerous areas on 5 weeks, nests of neoplastic cells and glandular cavity areas on 7 weeks, and nest areas of neoplastic cells on 9 and 11 weeks. The normalized intensities of Cer, CerP, and SM increase in glandular cavity during 3- to 7-week progression, and also experience several fluctuations in nests of neoplastic cells during tumor progression (Figure S4). All LPA, LPE, and PI show the spatiotemporal heterogeneity from 5 weeks, while PS do not exhibit heterogeneity, namely high abundances in the entire areas. Spatiotemporal heterogeneity of LPG (16:0), PE (38:2) and LPI occurs from 3, 5, and 9 weeks, respectively. For a detailed exhibition of all detected ion images and related information from different terminal times for tumor progression, see Figures 6 and S2–S5.

In addition, we select the total normalized intensities of three metabolites in multiple microareas during progression to structure the relationship between metabolite variation and tumor stiffness. We find that total normalized intensities of FA(22:4) and PI(38:4) positively correlate with their stiffness ($r = 0.491$, $P = 0.006$ for FA22:4, $r = 0.869$, $P < 0.001$ for PI(38:4)), and glycerophosphoinositol negatively correlate with their stiffness ($r = -0.386$, $P = 0.035$) (Figure S7).

Some sphingolipids (SPs) and glycerophospholipids (GPs), such as Cer, SM, PA, LPA, induce cancer cell-associated effects as extracellular messengers, such as cell proliferation, migration, angiogenesis, apoptosis, or metabolism.[40–42] Cer and SM are sphingolipid metabolites and messenger molecules that can be interconverted by sphingomyelinases and sphingomyelin synthase activities. Physiological actions of Cer in signal transduction include the promotion of cell cycle arrest and the induction of apoptosis. SM also acts as a lipid mediator to regulate cellular proliferation, migration, and inflammation. Similarly, as an inhibitor of apoptosis and a promoter of cell survival, ceramide 1-phosphate (CerP) is the product of Cer phosphorylation. CerP and Cer can transform into each other under ceramide kinase and lipid phosphatase activities. The regulation of Cer/SM balance, namely SM cycle, as well as the metabolic balance between Cer and CerP, are responsible for various cell functions and maintaining of

homeostasis of cell and tissue in tumor progression.[40−42] Our results display the dynamic variations of Cer, SM, and CerP in the SM-Cer signaling pathway from the spatiotemporal progression of breast tumor. CerP and SM are highly expressed in both nests of neoplastic cells and necrotic areas after 7-week progression, indicating that breast tumors from midlate stage progression have stronger invasion and metastasis potential.[40−42] We speculate that cellular molecule features show dynamic changes during the tumor progression, suggesting that heterogeneity of spatial distribution of molecules is a useful characteristic for evaluation of invasion or metastasis of tumor cells. It has been reported that PA significantly potentiated migration of breast cancer cells with high-grade invasion but had no disturbance on migration of either the nonneoplastic epithelial cells or noninvasive cancer cells, indicating the functional plasticity of lipids in tumor research.[43] Although lacking tumor progression-related spatiotemporal data, the LC−MS/MS-based analysis in some lipid species as described here has been previously found to be changed in breast cancer tissue.[44,45]

Taken as a whole, these data demonstrate that the spatiotemporal heterogeneity in physical characteristics and molecular metabolism exhibits obvious differences depending on the tumor progression. De novo FA synthesis during the tumor progression is independent and dependent on dietary FA intake. Specifically, FA species with various degrees of unsaturation show a significant upregulated in the core cancerous nest areas in the middle and late stages, while FA species with fully saturated lipids in the peripheral microareas in early stage, suggesting that these spatiotemporal features may be closely correlated with increased tumor proliferation and invasion, as well as the decreased permeability to drugs, respectively. Meanwhile, spatiotemporal heterogeneity of lipids from SM-Cer signaling pathway and GPs biosynthesis and degradation, as well as glycerophosphoinositol, occurs with increasing tumor progression. The result may be relevant to the upregulated abilities of migration and invasion of cancer cells. We also propose that spatiotemporal features of metabolites are a powerful tool for analysis and manipulation of tumor progression. According to the experimental results, glycerophosinositol, saturated FA, PA, Cer, CerP, SM, and LPG exhibit heterogeneous distribution in early stage, which may be suitable for early diagnosis markers in breast cancer. Representative LPI is abundant in the necrotic areas in the late stage (9 weeks). It is assumed that assessment of necrosis degree by using LPI distribution can serve as a powerful prognostic marker for breast cancer.

3. CONCLUSIONS

In summary, we developed a novel noninvasive UEg-MSI strategy that combines both physical characteristics and metabolic fingerprints at spatiotemporal level and allows us to use these properties as the periodical markers for tumor progression. The heuristic choice of elastic characteristics that primarily aims to improve the accuracy of tumor diagnosis in multifocal tumor progression ensures the integrity of in vivo data from tumor progression. Our precise features analysis reveals a diversity of spatiotemporal features that are anticipated to have potential clinical value for breast cancer, including the integrated investigation from in vivo and in vitro imaging, multifocal breast tumor progression, histopathological progression of breast tumor, and metabolic reprogramming, which allow us to describe different stages of tumor

progression and eventually explain or eradicate the resistance to cancer therapies. UEg-MSI also shows a great potential for the combination of cell mechanics and metabolic reprogramming. Additionally, these findings at multiple serial points in time also provide the potential forecasting capability for estimating the future developed state of cancer, such as invasive carcinoma and metastatic disease. Above all, our work represents a high-performance and clinically translatable technique for tumor progression by integrating physical characteristics, histopathological characteristics, and molecular imaging.

4. EXPERIMENTAL SECTION

4.1. Transgenic Animal Model of Breast Cancer Progression

All animal experiments are approved by the Shenzhen Institute of Advanced Technology (SIAT), Chinese Academy of Sciences (CAS) (Shenzhen, China) under protocol number SIAT-IACU-C-200330-YGS-ZC-A1228 and are conducted in accordance with the requirements of the Institutional Animal Care and Use Committee of SIAT, CAS. A transgenic mouse model, namely FVB/NJGpt-Tg (MMTV-PyMT), is established by breeding pairs purchased from Jackson Lab. and is used for breast tumor progression. MMTV plays an important role in the generation and development of mouse breast tumors. Using its functions including tissue-specific promoter and enhancer, it mediates the overexpression of oncogenes (such as PyMT, erbB2) in mammary gland and induces the rapid generation of multifocal mammary adenocarcinomas. We use MMTV-long terminal repeat (LTR) to drive the expression of polyomavirus middle T antigen (PyMT) in mouse mammary gland tissue, leading to the appearance of phenotype of breast tumor.[24−26] The 10 tumor primary foci including 1#, 2#, 3#, 4# and 5# were paired in five positions on both sides of the mouse. Ten tumor primary foci were monitored in each mouse. To avoid the effects of multiple anesthesia on tumor progression and potential metastasis during each ultrasound and UE and to satisfy the in vitro and in vivo imaging experiments, we did not choose the same group of mice to measure at five different time points. Five groups of female mice with multifocal breast tumors at three stages of tumor progression, respectively (early stage: 3 weeks; middle stage: 5 and 7 weeks; late stage: 9 and 11 weeks; 20 mice/group),[24−26] are analyzed by in vivo and in vitro imaging. In vivo imaging includes UE and ultrasound. In vitro imaging includes HE staining, MSI, and gene expression analysis.

4.2. Ultrasound Elastography

MMTV-PyMT mice are investigated by ultrasonic monitor at five points in time of tumor progression including 3, 5, 7, 9, and 11 weeks. B-mode and UE data are acquired using a Logic E9 ultrasonic diagnostic system (GE Healthcare, Chicago, IL, USA) with a linear array transducer at 6.0−15.0 MHz. Also of note, all the ultrasonic data are collected by the same operator following the standard diagnostic strategy for tumor monitoring, identification, measurement, and data acquisition. Meanwhile, five other operators are selected to verify ultrasound and UE results. Specifically, in order to avoid any impact on ultrasonic analysis, the abdominal wall of the mouse is depilated completely. Mice are kept anesthetized with isoflurane (2%) in 2.0 L/min of oxygen on a heated platform. Limbs of mouse are fixed on the plate, and a thick layer of prewarmed ultrasound coupling gel is coated on the surface of abdominal wall completely. Multiple tumors and their peripheral tissues are scanned using conventional B-mode scanning, screening the primary malignant focus, and measuring the maximal size at different growth stages of breast cancer. We set ROI for tumor analysis and collected the ultrasonic features, such as position, shape, echogenicity, tumor margin, to be more specific, the top and bottom of ROI included the subcutaneous adipose tissue and pectoral muscle, respectively, and the lateral borders are set more than 5 mm from the edge of tumor. For each mouse, the position of

transducer focus is arranged at the tumor center depth and remained consistent during all of the animal experiments.

When the collection of B-mode ultrasonic images was completed, it was switched to the UE mode at the maximal diameter plane of tumors, and targeted compression and decompression operations were implemented by a probe equipped with a 6−15 MHz linear array transducer. Namely, the operator can detect the proper pressure by monitoring the real-time elasticity variation while moving the probe. In the process of compression and decompression, the press indicator, displayed in red-yellow-green representing low-intermediate-high quality, respectively, is able to dynamically evaluate the quality of the UE. Guided by the quality bar, the elasticity data including grayscale and UE images are obtained using the real-time image mode with a 15 frames/s by optimizing operation. It is worth noting that the ROI of UE should be enlarged to include target tumors (area A) and peripheral tissue (area B) at the same depth, with at least 5 mm of distance from the boundary of the tumor to the lateral borders. Area A and area B are selected at the same frame, depth, and size. Strain ratio (SR) on elastography is achieved by the reference tissue (such as peripheral microarea of target tumors) strain divided by tumor strain, namely $SR = \text{Mean strain}_{\text{tumor peripheral tissue ROI, }d_x}/\text{Mean strain}_{\text{tumor ROI, }d_x}$ (d_x represents selected ROIs with the equal depths in normal or tumor tissue). SR can be automatically calculated by the ultrasonic diagnostic system after the operator confirms area A and area B. Each tumor is assessed at least eight times, and SR on elastography and elasticity score is recorded at each tumor. On the basis of the overall imaging pattern, an elasticity score on a five-point scale is used to evaluate the elasticity image of tumor according to the variation of color pattern both in the primary focus and peripheral area.[16,27] Briefly, score 1 indicates the distribution of soft strain with the entire hypoechoic lesion colored in green. Score 2 indicates the inhomogeneous distribution of strain with mosaic patterns of green and blue. Score 3 indicates the strain at the periphery of hypoechoic lesion (green), with sparing of the center of lesion (blue or mainly blue). Score 4 indicates a stiff strain in the central area (blue) except for the periphery area. Score 5 indicates a stiff strain in the entire hypoechoic lesion and the periphery area (blue).[16,27] A higher score indicates a higher malignancy degree of tumor. Five other operators are selected to verify the UE and elasticity score results. After UE and US, mice are immediately sacrificed at each imaging point in time, and tumor sections are collected for MSI and histopathological analysis.

4.3. Histopathological Imaging

Histopathological analysis protocol of breast tumor refers to the approach described by Zhao et al.[46] with minor modifications. Tumors from five points in time of progression are frozen into optimal cutting temperature compound by semiembedding approach and sliced into 10 μm sections. Tumor sections are stained with hematoxylin and eosin (H & E) to investigate the histopathological variation during the tumor progression. The critical dyeing time includes 4 min nuclear stain with hematoxylin and 45-s cytoplasm stain with eosin. Staining situation is observed by using Leica DM 2500 microscope (Leica, Germany). Histopathological images are achieved by using a digital pathology slide scanner (Aperio GT450, Leica, Germany). The morphological characteristics and areas of glandular cavity, necrosis, and nests of neoplastic cells are quantified by using Image-Pro Plus software (Version 6.0, Media cybernetics, USA) at 2× or 10× magnification.

4.4. MALDI-2 Imaging

Protocol of MSI for breast tumor progression refers to the approach described by Zhao et al.[47] with modifications. Tumor samples from different stages of progression are stored frozen at −80 °C, sectioned at 14 μm thickness using cryostat (CryoStar Nx70, Thermo Fisher Scientific, Germany) at −22 °C, thaw-mounted onto ITO conductive IntelliSlide (Bruker Daltonics, Bremen, Germany), and dried at 40 min by using vacuum desiccator before the MSI experiments. Matrix solution is prepared for 1,5-diaminonaphthalene (matrix substance for MALDI-MS, ≥99.0% HPLC, Sigma-Aldrich, USA) (20 mg/mL, 90:10, ACN:H_2O) and sprayed by using TM Sprayer (HTX Technologies, USA) with a nozzle temperature of 70 °C, nozzle

velocity of 1000 mm/min, solvent flow rate of 0.12 mL/min, pressure of 10 psi, and track spacing of 2 mm. MSI analysis is performed by using timsTOF flex MALDI-2 (Bruker Daltonics) platform with postionization, ion mobility collection, and MS/MS imaging function. The optimized conditions include the detection range of metabolite, m/z 100−900 Da; ion mode, negative; spatial resolution, 50 μm; range of ion mobility $1/K_0$ (V·s/cm^2), 0.6−1.7; laser frequency, 10,000 Hz; laser energy, 44%; laser shots, 350. Turn on postionization: the optimum value of the postionization laser energy, $\sim$ 200 μJ; triger delay, 10 μs for lipid molecules; smartbearm parameter, single M2; laser frequency, 1000 Hz; laser energy, 85%; laser shots, 30. For MS/MS imaging on tissue, the laser energy (88%) and shots (1000) are increased to generate high fragment yields of metabolites and high number of precursor ions at the ROIs in tumor sections.

After acquisition, raw data of MSI are imported and processed by using SCiLS Lab (2023a Pro, Bruker Daltonics). The standard pipelines of data processing include the denoising (weak), alignment, normalization of total ion count, segmentation, multivariable statistics (pLSA with deterministic initialization from component analysis), and visualization of ion images. Quantitative analysis of ions in ROIs is performed by using a SCiLS Lab and Metaboscape workstation (Bruker Daltonics). Box plots indicate the normalized intensity levels of metabolites in the specific microareas including the glandular cavity ("gc" and "hy+gc"), nests of neoplastic cells ("nc", "c", "c1" and "c2"), and necrotic areas ("n") during breast tumor progression. Lower and upper boundaries of the box indicate the first and third quartiles, respectively. The line within each notch box represents the median. Error bars represent the 1.5-fold interquartile range. Annotation and identification of metabolites are performed by comparing the actual m/z with theoretical m/z (relative errors of m/z < 2 ppm) sourced from MS-Metabase 3.0 database (Bruker Daltonics).

4.5. Gene Expression Analysis

Real time-quantitative polymerase chain reaction (RT-qPCR) experiments are carried out as described by Zhao et al.[48] The primer sequences are as follows: Fasn, forward 5′-ATGGATTACC-CAAGCGGTCT-3′ and reverse 5′-CCTGTCTCTGAGCCCTT-GAT-3′; Gapdh, forward 5′-AGGTCGGTGTGAACGGATTTG-3′ and 5′-GGGGTCGTTGA TGGCAACA-3′.

4.6. Statistical Analysis

All statistical analyses were performed using SPSS software. Repetitive measurements are analyzed by using means ± standard error of the means. The t test is applied to compare the differences in the Fasn expression, increased SR, the area of glandular cavity, nests of neoplastic cells and necrosis, as well as the normalized intensity levels of metabolites in the specific microareas during breast tumor progression. $P \leq 0.05$ is taken to be statistically significant. Spearman's correlation test is used to investigate the correlation between the variation of elasticity score and tumor volume and the correlation between the area of necrosis and increased SR during tumor progression. ROC curves and corresponding AUC with 95% confidence intervals are constructed and calculated to assess the performance of UE and conventional sonography in different progression of tumors, as well as UE performance for differentiating the early-stage, middle-stage, and late-stage tumors. Box plots in Figure 3 are used to show the histopathological characteristics during breast tumor progression, including the area variation of glandular cavity, nests of neoplastic cells, and necrosis. More details are indicated in figure legends.

■ ASSOCIATED CONTENT

Data Availability Statement

The data that support the findings of this study are available from the corresponding author upon reasonable request.

Ⓢ Supporting Information

The Supporting Information is available free of charge at https://pubs.acs.org/doi/10.1021/jacsau.3c00589.

Component analysis; coregistered information; spatio-temporal heterogeneity of metabolites; MS^2 spectrum of some metabolites; intensity analysis of metabolites; expression variation of Fasn; correlation between intensities and tumor stiffness; and metabolite information list (PDF)

■ AUTHOR INFORMATION

Corresponding Author

Chao Zhao − *Bionic Sensing and Intelligence Center, Institute of Biomedical and Health Engineering and Shenzhen Key Laboratory of Precision Diagnosis and Treatment of Depression, Shenzhen Institute of Advanced Technology, Chinese Academy of Sciences, Shenzhen 518055, China; Department of Ultrasound, First Affiliated Hospital of Shenzhen University Health Science Center, Shenzhen Second People's Hospital, Shenzhen 518009, China; University of Chinese Academy of Sciences, Beijing 100049, China;* ⊙ orcid.org/0000-0002-1765-6423; Email: chao.zhao@siat.ac.cn

Authors

Peng Zhou − *Bionic Sensing and Intelligence Center, Institute of Biomedical and Health Engineering, Shenzhen Institute of Advanced Technology, Chinese Academy of Sciences, Shenzhen 518055, China; Department of Ultrasound, First Affiliated Hospital of Shenzhen University Health Science Center, Shenzhen Second People's Hospital, Shenzhen 518009, China*

Yu Xiao − *Department of Thyroid and Breast department, First Affiliated Hospital of Shenzhen University, Shenzhen Second People's Hospital, Shenzhen 518009, China*

Xin Zhou − *Bionic Sensing and Intelligence Center, Institute of Biomedical and Health Engineering, Shenzhen Institute of Advanced Technology, Chinese Academy of Sciences, Shenzhen 518055, China*

Jinghui Fang − *Department of Ultrasound, First Affiliated Hospital of Shenzhen University Health Science Center, Shenzhen Second People's Hospital, Shenzhen 518009, China*

Jingwen Zhang − *Department of Ultrasound, First Affiliated Hospital of Shenzhen University Health Science Center, Shenzhen Second People's Hospital, Shenzhen 518009, China*

Jianjun Liu − *Shenzhen Key Laboratory of Modern Toxicology, Shenzhen Medical Key Discipline of Health Toxicology (2020-2024), Shenzhen Center for Disease Control and Prevention, 518054 Shenzhen, China*

Ling Guo − *Shenzhen Key Laboratory of Epigenetics and Precision Medicine for Cancers, National Cancer Center/ National Clinical Research Center for Cancer/Cancer Hospital & Shenzhen Hospital, Chinese Academic of Medical Sciences & Peking Union Medical College, Shenzhen 518172, China*

Jiuhong Zhang − *Shenzhen Key Laboratory of Modern Toxicology, Shenzhen Medical Key Discipline of Health Toxicology (2020-2024), Shenzhen Center for Disease Control and Prevention, 518054 Shenzhen, China*

Ning Zhang − *College of Chemistry and Chemical Engineering, Dezhou University, Dezhou 253026 Shandong, China;* ⊙ orcid.org/0000-0002-6161-5469

Ke Chen − *Key Laboratory of Resources Conversion and Pollution Control of the State Ethnic Affairs Commission, College of Resources and Environmental Science, South-Central Minzu University, Wuhan 430074, China*

Complete contact information is available at:
https://pubs.acs.org/10.1021/jacsau.3c00589

Author Contributions

¶P.Z. and Y.X. are co-first author.

Author Contributions

P.Z. and Y.X. contributed equally to this work. C.Z., P.Z., and Y.X. planned this work and designed the research method. P.Z., Y.X., X.Z., J.F., and J.Z. contributed to UE and ultrasound imaging in the mouse model. C.Z., Y.X., X.Z., J.L., L.G., J.Z., N.Z., and K.C. contributed to MSI, histopathological imaging, and statistical analysis. C.Z., P.Z., and Y.X. cowrote the manuscript and analyzed the data. C.Z. supervised and directed the study.

Notes

The authors declare no competing financial interest.

■ REFERENCES

(1) Harbeck, N.; Penault-Llorca, F.; Cortes, J.; et al. Breast cancer. *Nat. Rev. Dis. Primers* **2019**, *5*, 66.

(2) Nik-Zainal, S.; Davies, H.; Staaf, J.; et al. Landscape of somatic mutations in 560 breast cancer whole-genome sequences. *Nature.* **2016**, *534*, 47.

(3) Rothé, F.; Venet, D.; Peeters, D.; et al. Interrogating breast cancer heterogeneity using single and pooled circulating tumor cell analysis. *npj Breast Cancer* **2022**, *8*, 79.

(4) Pasha, N.; Turner, N. C. Understanding and overcoming tumor heterogeneity in metastatic breast cancer treatment. *Nat. Cancer.* **2021**, *2*, 680.

(5) Andersson, A.; Larsson, L.; Stenbeck, L.; et al. Spatial deconvolution of HER2-positive breast cancer delineates tumor-associated cell type interactions. *Nat. Commun.* **2021**, *14*, 6012.

(6) Alizadeh, A. A.; Aranda, V.; Bardelli, A.; et al. Toward understanding and exploiting tumor heterogeneity. *Nat. Med.* **2015**, *21*, 846.

(7) Kim, J.; DeBerardinis, R. J. Mechanisms and implications of metabolic heterogeneity in cancer. *Cell Metab.* **2019**, *30*, 434.

(8) Gallaher, J. A.; Enriquez-Navas, P. M.; Luddy, K. A.; et al. Spatial heterogeneity and evolutionary dynamics modulate time to recurrence

in continuous and adaptive cancer therapies. *Cancer Res.* **2018**, *78*, 2127.

(9) Rinschen, M. M.; Ivanisevic, J.; Giera, M.; et al. Identification of bioactive metabolites using activity metabolomics. *Nat. Rev. Mol. Cell Bio.* **2019**, *20*, 353.

(10) Lai, Y. H.; Wang, Y. S. Advances in high-resolution mass spectrometry techniques for analysis of high mass-to-charge ions. *Mass Spectrom. Rev.* **2023**, *42*, 2426.

(11) Vidavsky, N.; Kunitake, J. A. M. R.; Diaz-Rubio, M. E.; Chiou, A. E.; Loh, H.; Zhang, S.; Masic, A.; Fischbach, C.; Estroff, L. A. Mapping and profiling lipid distribution in a 3D model of breast cancer progression. *ACS Cen. Sci.* **2019**, *5*, 768−780.

(12) Sun, C. L.; Wang, A. Q.; Zhou, Y. H.; et al. Spatially resolved multi-omics highlights cell-specific metabolic remodeling and interactions in gastric cancer. *Nat. Commun.* **2023**, *14*, 2692.

(13) Zhao, C.; Guo, L.; Dong, J. Y.; et al. Mass spectrometry imaging-based multi-modal technique: next-generation of biochemical analysis strategy. *Innovation* **2021**, *2*, No. 100151.

(14) Santoro, A. L.; Drummond, R. D.; Silva, I. T.; et al. In situ DESI-MSI lipidomic profiles of breast cancer molecular subtypes and precursor lesions. *Cancer Res.* **2020**, *80*, 1246.

(15) Kawashima, M.; Tokiwa, M.; Nishimura, T. High-resolution imaging mass spectrometry combined with transcriptomic analysis identified a link between fatty acid composition of phosphatidylino-sitols and the immune checkpoint pathway at the primary tumour site of breast cancer. *Br. J. Cancer* **2020**, *122*, 245.

(16) Faruk, T.; Islam, M. K.; Arefin, S.; et al. The journey of elastography: background, current status, and future possibilities in breast cancer diagnosis. *Clin. Breast Cancer* **2015**, *15*, 313.

(17) Rix, A.; Piepenbrock, M.; Flege, B.; et al. (2021), Effects of contrast-enhanced ultrasound treatment on neoadjuvant chemo-therapy in breast cancer. *Theranostics* **2021**, *11*, 9557.

(18) Ma, Y.; Zhang, S.; Zang, L.; et al. Combination of shear wave elastography and Ki-67 index as a novel predictive modality for the pathological response to neoadjuvant chemotherapy in patients with invasive breast cancer. *Eur. J. Cancer* **2016**, *69*, 86.

(19) Fernandes, J.; Sannachi, L.; Tran, W. T.; et al. Monitoring breast cancer response to neoadjuvant chemotherapy using ultrasound strain elastography, monitoring breast cancer response to neoadjuvant chemotherapy using ultrasound strain elastography. *Transl. Oncol.* **2019**, *12*, 1177.

(20) Evans, A.; Armstrong, S.; Whelehan, P.; et al. Can shear-wave elastography predict response to neoadjuvant chemotherapy in women with invasive breast cancer? *Br. J. Cancer* **2013**, *109*, 2798.

(21) Wang, J. W.; Guo, Z. X.; Lin, Q. G.; et al. Ultrasound elastography as an imaging biomarker for detection of early tumor response to chemotherapy in a murine breast cancer model: a feasibility study. *Br. J. Radiol.* **2018**, *91*, No. 20170698.

(22) Sun, J.; Cai, J.; Wang, X. Real-time ultrasound elastography for differentiation of benign and malignant thyroid nodules: a meta-analysis. *J. Ultrasound Med.* **2014**, *33*, 495.

(23) Lan, L.; Feng, K.; Wu, Y.; Zhang, W.; Wei, L.; Che, H.; Xue, L.; Gao, Y.; Tao, J.; Qian, S.; Cao, W.; Zhang, J.; Wang, C.; Tian, M. Phenomic imaging. *Phenomics.* **2023**, *3*, 597.

(24) Herschkowitz, J. I.; Simin, K.; Weigman, V. J.; et al. Identification of conserved gene expression features between murine mammary carcinoma models and human breast tumors. *Genome Biol.* **2007**, *8*, R76.

(25) Dilworth, S. M. Polyoma virus middle T antigen and its role in identifying cancer-related molecules. *Nat. Rev. Cancer* **2002**, *2*, 951.

(26) Attalla, S.; Taifour, T.; Bui, T.; et al. Insights from transgenic mouse models of PyMT-induced breast cancer: recapitulating human breast cancer progression in vivo. *Oncogene* **2021**, *40*, 475.

(27) Itoh, A.; Ueno, E.; Tohno, E.; et al. Breast disease: clinical application of US elastography for diagnosis. *Radiology* **2006**, *239*, 341.

(28) Romani, P.; Valcarcel-Jimenez, L.; Frezza, C.; et al. Crosstalk between mechanotransduction and metabolism, crosstalk between mechanotransduction and metabolism. *Nat. Rev. Mol. Cell Biol.* **2021**, *22*, 22.

(29) Cairns, R. A.; Harris, I. S.; Mak, T. W. Regulation of cancer cell metabolism. *Nat. Rev. Cancer* **2011**, *11*, 85.

(30) Ackerman, D.; Simon, M. C. Hypoxia, lipids, and cancer: surviving the harsh tumor microenvironment. *Trends Cell Biol.* **2014**, *24*, 472.

(31) Abdelmoula, W. M.; Balluff, B.; Englert, S.; et al. Data-driven identification of prognostic tumor subpopulations using spatially mapped t-SNE of mass spectrometry imaging data. *P. Natl. Acad. Sci. U.S.A.* **2016**, *113*, 12244.

(32) Guo, L.; Dong, J. Y.; Xu, X. N.; et al. Divide and conquer: a flexible deep learning strategy for exploring metabolic heterogeneity from mass spectrometry imaging data. *Anal. Chem.* **2023**, *95*, 1924.

(33) Buccione, R.; Baldassarre, M.; Trapani, V.; et al. Glycer-ophosphoinositols inhibit the ability of tumour cells to invade the extracellular matrix. *Eur. J. Cancer* **2005**, *41*, 470.

(34) Corda, D.; Zizza, P.; Varone, A. The glycerophosphoinositols: cellular metabolism and biological functions. *Cell. Mol. Life Sci.* **2009**, *66*, 3449.

(35) Corda, D.; Iurisci, C.; Berrie, C. P. Biological activities and metabolism of the lysophosphoinositides and glycerophosphoinosi-tols. *Biochim. Biophys. Acta* **2002**, *1582*, 52.

(36) You, M. S.; Xie, Z. L.; Zhang, N. Signaling pathways in cancer metabolism: mechanisms and therapeutic targets. *Signal Transduction Targeted Ther.* **2023**, *8*, 196.

(37) Koundouros, N.; Poulogiannis, G. Reprogramming of fatty acid metabolism in cancer. *Br. J. Cancer* **2020**, *122*, 4.

(38) Kuhajda, F. P.; Pizer, E. S.; Li, J. N. Synthesis and antitumor activity of an inhibitor of fatty acid synthase. *Proc. Natl. Acad. Sci. U. S. A.* **2000**, *97*, 3450.

(39) Rysman, E.; Brusselmans, K.; Scheys, K. *De novo* lipogenesis protects cancer cells from free radicals and chemotherapeutics by promoting membrane lipid saturation. *Cancer Res.* **2010**, *70*, 8117.

(40) Morad, S. A. F.; Cabot, M. C. Ceramide-orchestrated signalling in cancer cells. *Nat. Rev. Cancer* **2013**, *13*, 51.

(41) Paolo, G. D.; Camilli, P. D. Phosphoinositides in cell regulation and membrane dynamics. *Nature* **2006**, *443*, 651.

(42) Ponnusamy, S.; Meyers-Needham, M.; Senkal, C. E. Sphingolipids and cancer: ceramide and sphingosine-1-phosphate in the regulation of cell death and drug resistance. *Future Oncol.* **2010**, *6*, 1603.

(43) Sliva, D.; Mason, R.; Xiao, H.; et al. Enhancement of the migration of metastatic human breast cancer cells by phosphatidic acid. *Biochem. Biophys. Res. Commun.* **2000**, *268*, 471.

(44) Moro, K.; Kawaguchi, T.; Tsuchida, J.; et al. Ceramide species are elevated in human breast cancer and are associated with less aggressiveness. *Oncotarget* **2018**, *9*, 19874.

(45) Schiffmann, S.; Sandner, J.; Birod, K.; et al. Ceramide synthases and ceramide levels are increased in breast cancer tissue. *Carcino-genesis* **2009**, *30*, 745.

(46) Zhao, C.; Xie, P. S.; Yong, T.; et al. Airborne fine particulate matter induces cognitive and emotional disorders in offspring mice exposed during pregnancy. *Sci. Bull.* **2021**, *66*, 578.

(47) Zhao, C.; Yong, T.; Zhang, Y. B.; et al. Breast cancer proliferation and deterioration-associated metabolic heterogeneity changes induced by exposure of bisphenol S, a widespread replacement of bisphenol A. *J. Haz. Mater.* **2021**, *414*, No. 125391.

(48) Zhao, C.; Yong, T.; Zhang, Y. B.; et al. Evaluation of the splenic injury following exposure of mice to bisphenol S: a mass spectrometry-based lipidomics and imaging analysis. *Environ. Int.* **2020**, *135*, No. 105378.